Initial Buried Minehunting Demonstration of the Laser Scalar Gradiometer Operating Onboard REMUS 600

T. R. Clem[a], J. T. Bono[a], P. S. Davis[a], D. J. Overway[a], L. Vaizer[a],
D. King[b], A. Torres[b], T. Austin[c], R. P. Stokey[c], and G. Packard[c]

[a]Naval Surface Warfare Center, 110 Vernon Ave, Panama City, FL 32407, USA
[b]Polatomic, Inc., 1810 N. Glenville Dr. #116, Richardson TX 75081, USA
[c]Woods Hole Oceanographic Institution, Woods Hole, MA 02543, U.S.A.

Abstract - **The Laser Scalar Gradiometer (LSG) is a sensitive passive magnetic sensor based on the opto-magnetic properties of helium-4 gas in accordance with the Zeeman effect. The LSG has attained increased sensitivity over comparable sensors by the use of a laser in place of incoherent light for optical pumping. It employs four helium sense cells configured in a volume-filling arrangement to measure four independent channels of information: the scalar field magnitude and three linearly independent admixtures of the three components of the scalar-field gradient vector. The LSG has now been integrated into the REMUS 600 and evaluated in land-based testing. This land-based testing has assured the proper functionality of this integrated system prototype and established the sensor's noise floor in the electromagnetic environment of the REMUS 600. Following this land-based testing, at-sea shakedown tests and experiments over target fields have been conducted to provide a more definitive measure of the LSG's performance under actual operational conditions and to evaluate its current capability to detect, classify, and localize (DCL) buried mines. The system configuration, the experiment design, associated test procedures, and results of data analysis from the underwater experiments conducted with the LSG onboard REMUS 600 are reported in this paper.**

I - INTRODUCTION

The Office of Naval Research (ONR) has identified notional concepts for buried minehunting (BMH) operations and has developed advanced sensor capabilities for operation onboard Autonomous Underwater Vehicles (AUVs). The principal concept under investigation involves the use of AUV-based sonars such as the Small Synthetic Aperture Minehunter (SSAM) for long-range buried target search-classify-map (SCM) operations and AUV-based acoustic and non-acoustic sensors for subsequent reacquisition and identification (RI) of the SCM contacts at closer ranges. Focal RI sensors, which have been developed and are now being evaluated for BMH, are the Bottom Object Search Sonar (BOSS), the Realtime Tracking Gradiometer (RTG), and the Laser Scalar Gradiometer (LSG). In this paper, we will describe progress in the development and testing of the LSG. Additional papers have been published to describe parallel progress in the development and testing of SSAM [1], BOSS [2], and the RTG [3].

The LSG is a sensitive multi-channel electron-spin resonance passive scalar magnetometer-gradiometer based on the opto-magnetic properties of helium-4 gas in accordance with the Zeeman effect. The LSG and its predecessor, the P-2000, have attained increased sensitivity over comparable opto-magnetic sensors by the use of a laser in place of incoherent light for optical pumping [4],[5]. The LSG employs four helium sense cells configured in a volume-filling arrangement to measure four independent channels of information: the scalar field magnitude and admixtures of the three components of the scalar-field gradient vector from which the scalar-gradient vector can be constructed algebraically. The multi-channel approach employed in the LSG provides 3-dimensional localization and classification of the three components of the magnetic moment for a magnetic dipole target, a capability not offered by conventional single-channel scalar magnetometers.

The LSG is shown in Fig. 1 with its sense-cell assembly and electronics outside the container. The four-cell assembly is displayed and labeled in Fig. 1(b). This arrangement has been staggered so that it can conform to the 11-1/2" sensor housing (that, in turn, fits within the 12-3/4" AUV) and also provide sufficient cell-to-cell separation so that intra-cell crosstalk will not limit sensitivity. The coordinates for the centers of the four cells are provided in a right-handed coordinate system with origin at cell A, the x axis parallel to the axis of symmetry positive forward from the electronics toward the sense-cell assembly, y horizontal across axis, and z vertical positive down. In this coordinate system, the B, C, and D cells have the coordinates (0.162 m, 0 m, 0.177 m), (0.355 m, -0.109 m, 0.0884 m), and (0.454 m, 0.109 m, 0.0884 cm), respectively. For reference to Section III, the gradient baselines, i.e. the cell-to-cell distances, for all 6 cell pairs are L_{ab} = 0.240 m, L_{ac} = 0.382 m, L_{ad} = 0.475 m, L_{bc} = 0.239 m, L_{bd} = 0.324 m, and L_{cd} = 0.239 m.

The appearance of trade names in this document does not constitute endorsement by the Department of Defense; the Navy; or the Naval Surface Warfare Center.

1-4244-0115-1/06/$20.00 ©2006 IEEE

Report Documentation Page

Form Approved
OMB No. 0704-0188

1. REPORT DATE	2. REPORT TYPE	3. DATES COVERED
01 SEP 2006	**N/A**	**-**

4. TITLE AND SUBTITLE	5a. CONTRACT NUMBER
Initial Buried Minehunting Demonstration of the Laser Scalar Gradiometer Operating Onboard REMUS 600	5b. GRANT NUMBER
	5c. PROGRAM ELEMENT NUMBER
6. AUTHOR(S)	5d. PROJECT NUMBER
	5e. TASK NUMBER
	5f. WORK UNIT NUMBER
7. PERFORMING ORGANIZATION NAME(S) AND ADDRESS(ES) **Naval Surface Warfare Center, 110 Vernon Ave, Panama City, FL 32407, USA**	8. PERFORMING ORGANIZATION REPORT NUMBER
9. SPONSORING/MONITORING AGENCY NAME(S) AND ADDRESS(ES)	10. SPONSOR/MONITOR'S ACRONYM(S)
	11. SPONSOR/MONITOR'S REPORT NUMBER(S)

12. DISTRIBUTION/AVAILABILITY STATEMENT
Approved for public release, distribution unlimited

13. SUPPLEMENTARY NOTES
See also ADM002006. Proceedings of the MTS/IEEE OCEANS 2006 Boston Conference and Exhibition Held in Boston, Massachusetts on September 15-21, 2006, The original document contains color images.

14. ABSTRACT

15. SUBJECT TERMS

16. SECURITY CLASSIFICATION OF:			17. LIMITATION OF ABSTRACT	18. NUMBER OF PAGES	19a. NAME OF RESPONSIBLE PERSON
a. REPORT	b. ABSTRACT	c. THIS PAGE			
unclassified	**unclassified**	**unclassified**	**UU**	**7**	

Standard Form 298 (Rev. 8-98)
Prescribed by ANSI Std Z39-18

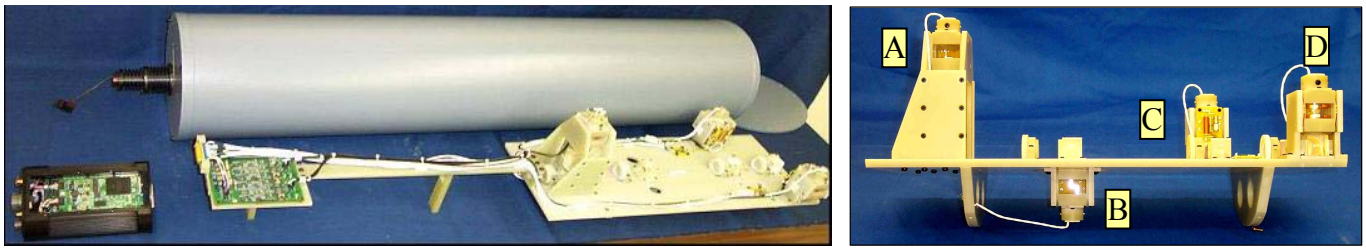

(a) (b)

Figure 1. Pictorial display of the LSG: (a) photograph displaying a side view of the LSG along with its major subassemblies outside of the container and (b) photograph of the four-cell sensor assembly.

To satisfy the size and power requirements for operation in small AUVs and the requirement for autonomous sensor operation, the LSG features integrated digital surface mount technology and integration of all of the system resonance loop electronics for the sensor unit into a package considerably smaller than the rack-mounted electronics employed in the P-2000. More details on the LSG design have been reported in Reference 5.

In initial testing, LSG performance has been measured while stationary and in motion in a magnetically quiet environment. Results of such testing conducted in 2005 are reported in Reference 5. Specifically, a gradient white noise of 8.3×10^{-3} nT/(m-Hz$^{1/2}$) operating stationary in a magnetically quiet environment was reported for one gradiometer with a baseline of 0.24 meters.

An LSG payload section has been assembled to interface the LSG with the REMUS 600 AUV (Fig. 2). Henceforth we will refer to this system prototype as the LSG-REMUS system. Basic design and features of the payload section, relevant features and capabilities of the REMUS 600, and important interface factors are discussed in Section II. Land-based testing of the LSG onboard REMUS 600 has been conducted to assure proper functionality of this integrated system prototype and to establish the LSG's noise floor in the electromagnetic environment of REMUS 600 with and without noise-cancellation using platform-monitoring ancillary sensors.

Following this land-based testing, underwater shakedown tests and experiments over target fields have been conducted to provide a more definitive measure of the performance of the LSG integrated with REMUS under actual operational conditions.

In preparation for these first sea tests, the primary detection/classification/localization (DCL) algorithm validated and used for tensor gradiometers such as the RTG over a period of years [6] has been modified to accommodate the scalar signals detected by the individual sense cells (in contrast to the vector signals for individual vector magnetometers commonly employed in tensor gradiometers such as the RTG). The effectiveness of this modified algorithm to localize and classify magnetic-dipole targets has been evaluated using data collected during the recent tests. The noise floor for LSG gradiometer channels in the current LSG-REMUS configuration under operational conditions and sample results of target DCL are reported in Section III.

II – DESCRIPTION OF THE LSG-REMUS SYSTEM CONFIGURATION

The LSG has now been interfaced with the REMUS 600, an AUV designed to support a wide variety of modular payloads via a standardized interface. REMUS 600 features an open two bladed propeller for propulsion and three independent control fins for attitude and navigational control [7]. The core vehicle has an outer diameter of 12.75 inches and a length of 73 inches prior to payload interface. It provides 28VDC power from the vehicle's polymer lithium ion battery packs and a 10 Base-T Ethernet connection. Precise underwater navigation is achieved via a Kearfott T-24 Inertial Navigation System (INS) and a RD Instruments 600 kHz phased-array Doppler Velocity Log (DVL). GPS fixes, obtained while the vehicle is on the surface, are merged with

Figure 2. Photograph of the LSG-REMUS system.

the data collected by the INS and DVL systems in order to estimate absolute vehicle position.

A dry payload and nose section has been assembled to interface the LSG with REMUS 600 for preliminary testing. Both the payload section and the nose are constructed from composite materials, more specifically eglass fibers in a vinyl-ester resin. If these components had been metallic, vehicle rotations in the Earth's magnetic field would induce eddy currents, which would have generated performance-limiting magnetic noise at the sensors. On the other hand, the rear bulkhead, which seals the payload section, is constructed from aluminum. Any induced magnetic noise arising from this bulkhead, when measured at the sensor assembly, is expected to be under the present noise floor. Waterproof connectors mounted in this bulkhead provide the necessary power and communications interface between the LSG and the AUV. The desired configuration is to house this payload section at the nose of the vehicle, ahead of any other possible payloads (not a factor for the current configuration) with the sensor subsystem positioned forward of its own electronics. This design philosophy maximizes the distance of the platform noise sources from the sensing elements.

The LSG payload has been integrated with REMUS 600 and basic mechanical, electrical, and communication interfaces have been established. The LSG-REMUS system has a length of 149 inches (Fig. 2). As a result of the relatively low packing density in the dry body section, ballast in the form of non-magnetic lead plate has been mounted in the body section to make it neutrally buoyant. LSG cooling is an issue for this configuration since the sensor is encapsulated by a thermally-insulating composite body section. An active thermoelectric cooling unit has been installed for the initial testing. Based on a thermal analysis conducted to assess cooling options [8], we currently plan to replace this active cooling unit with a passive cooling system prior to future tests of the LSG-REMUS system.

A second single-board computer, external to the LSG, has been integrated into the LSG payload section. This computer handles

a) LSG data management and storage;
b) Ethernet communications with the REMUS computer to provide LSG operational status to the REMUS computer and to log vehicle- and mission-related information from the REMUS computer;
c) the collection of serial data from the INS; and
d) real-time signal processing for target DCL (not yet implemented).

Three 3-axis fluxgate vector magnetometers and two current sensors distributed in the vehicle were employed as ancillary reference magnetometers to monitor and cancel platform magnetic noise for the testing and analysis reported in this study. Specifically, one Billingsley TFM 100G2 3-axis magnetometer [14] was mounted with a standard fixture on the rear bulkhead of the LSG with the LSG electronics and laser, one Applied Physics Systems Model 533 3-axis magnetometer was mounted in the REMUS electronics-battery section and a second Model 533 in the aft section housing the propulsion unit and the fin-control assembly. One LEM Components LA55-P current sensor measured the total battery current to all subsystems in the core vehicle and in the LSG payload; while one LEM Components LAH25-NP current sensor measured the currents to all core vehicle subsystems except the fin assembly and the propulsion system. Analog electronics mounted in the LSG payload section provided necessary voltage scaling to couple the analog signals from the ancillary sensors into LSG A/D converters.

III – LSG PERFORMANCE IN AT-SEA TESTING

At-sea testing of the LSG-REMUS system was conducted following system integration and land-based checkout. Specific goals of these tests

1) Evaluation of LSG performance when integrated with the REMUS 600 during underwater operational conditions, effectiveness of the navigational information and the vehicle control algorithms developed for the LSG-REMUS system for target reacquisition and assignment of absolute GPS coordinates to target localizations;
2) Collection of at-sea data with the sensor operating onboard REMUS 600 to test and refine the algorithms developed for noise cancellation and for target classification and localization;
3) Assessment of LSG performance against bottom mine-like targets located in drill target fields deployed in the Gulf of Mexico and in Saint Andrew Bay using algorithms developed in FY 2006; and
4) Use of the results of the testing and subsequent data analysis to identify and implement hardware and software modifications to enhance the LSG-REMUS system.

We will describe the results to measure LSG noise performance from our initial at-sea testing of the LSG-REMUS system in Subsection A. Results from the at-sea testing to localize and classify targets is described in Subsection B.

A. LSG Noise in the LSG-REMUS System

The principal measures of sensor performance reported for this investigation are the outputs from individual magnetometers and scalar gradients, which are defined as the difference of two magnetometer outputs divided by the baseline (where baseline is the distance between the selected magnetometers). The low-level noise characteristic of a sensitive magnetic sensor is essential for greater detection range, and is typically masked during mobile operation by a number of noise sources encountered outside of a laboratory environment. We generally use frequency-domain signal processing with standard Fast Fourier transform (FFT) techniques applied to linear systems with multiple inputs and multiple outputs subject to stationary random inputs [9]. At each frequency f, we form the compensated signal Y by subtracting the signal components that are correlated with relevant reference channels, such as fluxgate magnetometers and current sensors. The effectiveness of this approach is determined by the degree of coherence between the reference

sensors to the significant noise sources. Ideally, the compensated signal would be the intrinsic sensor noise obtained with the sensor operating stationary in a magnetically-quiet environment.

Results from our earlier land-based experiments to characterize the LSG's intrinsic performance were reported in Reference 5. A gradient white noise of 8×10^{-3} nT/(m-Hz$^{1/2}$) down to approximately 0.05 Hz with noise following a 1/f power law at lower frequencies was reported for one gradiometer with a baseline of 0.24 meters. This corresponds to a magnetometer white noise floor of 2×10^{-3} nT/Hz$^{1/2}$ for the differenced cell pair and a single-cell magnetometer white noise operated in differenced mode a factor of $1/\sqrt{2}$ smaller, i.e. 1.4×10^{-3} nT/Hz$^{1/2}$.

LSG noise operating in the current LSG-REMUS system configuration under nominal underwater operational conditions has been measured. These measurements were conducted in relatively deep waters (nominally 30 meters) in an area believed to be relatively free of any significant magnetic clutter on the bottom such as sunken ships. The measurements were conducted while the system ran at a constant depth of 6 meters; i.e., at a nominal altitude of 24 meters off the bottom. This measurement was conducted at a high altitude to minimize signals from magnetic clutter on the bottom. The system ran at a nominal speed of 4 Knots. Data were collected as the system traversed two square noise boxes with legs one nautical mile in length. The first box consisted of two legs parallel to a north-south heading and two legs parallel to an east-west heading. The second box was rotated 45° around the center point for the first square; i.e., it consisted of two legs parallel to a NE-to-SW heading and two legs parallel to a NW-to-SE line.

Both gradient and field spectra, from data collected during one of these legs, are displayed in Fig. 3. The results for all six LSG gradiometer channels, synthesized by differencing each pair of LSG magnetometers, are displayed in Fig. 3(a). With the exception of the B-C case, the raw gradients displayed similar amplitudes and followed a power law approaching $1/f^2$ in the frequency band of 0.1 up to 10 Hz although more individual behavior was observed for the gradients at frequencies lower than 0.1 Hz.

The frequency-domain noise cancellation approach was employed using the three 3-axis fluxgate magnetometers and the two current sensors described in Section II as reference channels. Several interesting trends were observed from the results. First, the C-D gradient had the lowest noise floor ranging from 4×10^{-2} down to 2×10^{-2} nT/(m-Hz$^{1/2}$) in the band from 0.02 to 1 Hz, a fact not surprising since C and D are the two magnetometers most removed from the platform magnetic noise in the rear of the vehicle. The corresponding noise figure for the C-D differenced magnetometer was 1×10^{-2} down to 5×10^{-3} nT/Hz$^{1/2}$ in the same frequency band. 10-to-20 dB noise cancellation was realized for this gradient with the noise cancellation increasing at the lower frequencies.

Not surprisingly, the noise floor increased for the two gradients using cell B as the aft-most magnetometer, and the noise floor was elevated the most for those gradients using cell A, the aft-most magnetometer. The results for B-C and B-D were nearly identical, displaying amplitudes from 1×10^{-1} down to 5×10^{-2} nT/(m-Hz$^{1/2}$) in the frequency band from 0.02 to 1 Hz. Finally, the results for A-B, A-C, and A-D were also nearly identical, displaying amplitudes from 1.2×10^{-1} down to 5×10^{-2} nT/(m-Hz$^{1/2}$) in the band from 0.02 to 1 Hz.

The raw field signals for all four magnetometers are shown in Fig. 3(b). They display similar amplitudes and followed a power law approaching $1/f^2$ in the frequency band of 0.1 up to 10 Hz. The A, B, and C magnetometers displayed similar growth at lower frequencies. Surprisingly, the field value for the A magnetometer was somewhat lower than the others at frequencies below 0.1 Hz.

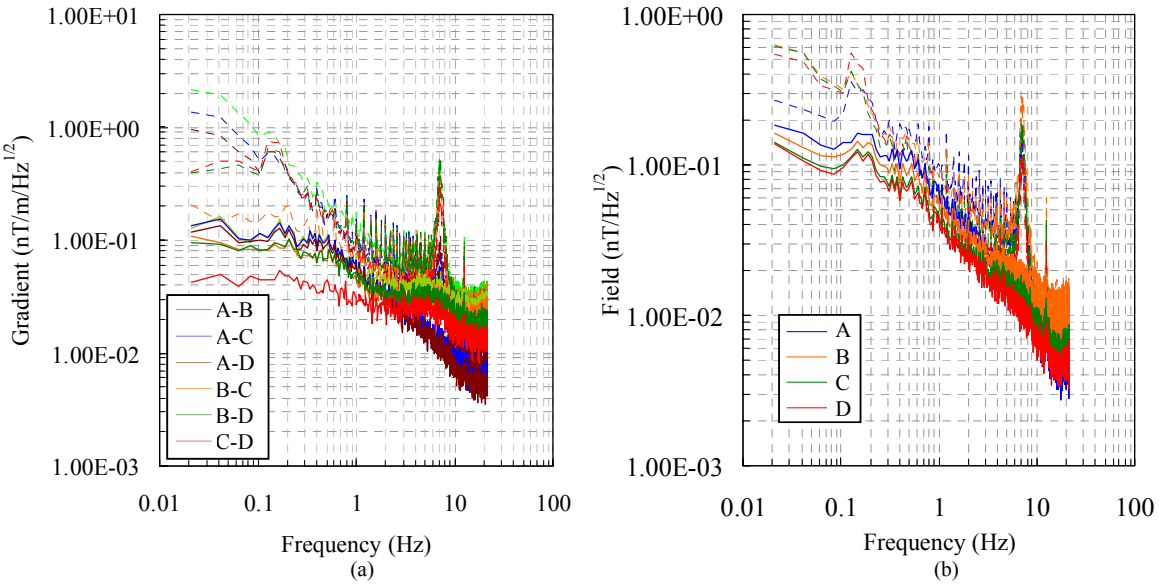

Figure 3. Amplitude spectrums obtained during sea testing of the LSG-REMUS system for (a) gradient and (b) field.

The frequency-domain noise cancellation approach was also employed for these magnetometers, again using the three 3-axis fluxgate magnetometers and two current sensors as references. Several interesting trends were observed from the results. First, the D magnetometer had the lowest noise floor ranging from 1.5 $x10^{-1}$ down to $4x10^{-2}$ $nT/Hz^{1/2}$ in the band from 0.02 to 0.3 Hz, a fact not surprising since the D sensor is most removed from the platform electromagnetic noise in the rear of the vehicle. For this case, only 6-to-12 dB noise cancellation was observed in the range from 0.02 to 0.3 Hz, with the noise cancellation improving at the lower frequencies. Negligible compensation was observed at higher frequencies. Not surprisingly, the noise floor increased as the magnetometer got closer to the platform magnetic noise sources aft of the LSG sensor although the increased noise was not striking.

B – Target Localization

The Vaizer-Lathrop-Bono (VLB) technique provides a windowed-data statistical-fitting technique for the DCL of magnetic targets. This technique was first developed for five-channel tensor gradiometers and successfully validated in the MADOM project [6]. The algorithms for tensor gradiometers have been exercised with fewer than five tensor-gradient channels and have demonstrated reasonable results even when as few as three channels are used. For the LSG, there are four independent channels of information: the scalar magnetic field and three independent scalar-gradient components synthesized by differencing three appropriately chosen pairs of scalar magnetometer channels. The VLB DCL algorithm has been modified to fit LSG data to these model scalar field and scalar gradient signals and has been validated via simulation for application to the LSG. An abbreviated description of the algorithm is given in Reference 5.

This represents the first test of the algorithm using sensor data collected against targets in the underwater environment. For this data analysis, LSG data was low-pass filtered at 2 Hz and merged with REMUS navigation data. LSG magnetic and REMUS navigation data were aligned by correlating estimated LSG rotations in the Earth's magnetic field and INS measurements of roll, pitch and yaw. LSG data was segmented to extract sections of interest and run through the LSG localization algorithm. As discussed in Section II, three 3-axis fluxgate magnetometers and two current meters installed in different sections of the vehicle were used to monitor and cancel the effects of motion- and vehicle-generated magnetic noise. A more complete description of the algorithm and its performance will be reported once the algorithm has been fully validated.

An example of LSG target localization is displayed in Fig. 4 for six tracks past three identical ferrous-case cylindrical targets with a length 3.5 meters and a diameter of 0.5 meters. These targets were deployed by divers nominally in the same orientation, with a target-to-target spacing of approximately 300 meters. The localization predictions are plotted on top of the REMUS tracks and color-coded to the corresponding track. Ground-truth positions for targets T1, T2, and T3 are displayed by black icons. Although it is not an important factor for magnetic target detection, T1 was proud to the bottom, T2 half buried, and T3 fully buried. The tracks have been spatially rotated into a horizontal orientation for better visualization of the localization results. This survey was conducted at a constant altitude of 5 meters (nominal depth of 15 meters) and at a speed of 4 Knots. Only the localization results with sufficiently high confidence have been plotted. All three targets were detected and localized with sufficient confidence on five out of six runs. On the sixth run, the three targets were detected at the expected along-track CPA positions, but the confidence was below the accepted threshold.

The relative target-to-target positions within a single track as predicted by the LSG localization algorithm cluster very well to within a spatial translation with predictions made for the other tracks and with ground-truth measurements. At least some of the run-to-run variation can be explained by navigation errors accumulated during the mission (in this case conducted with GPS fixes only at the initiation and completion of the 6-track mission). In order to estimate the accuracy of the track-to-track relative localizations, we calculated the position differences for along-track Δx and cross-track Δy variations between T1 and T2 and between T1 and T3. The Δx and Δy standard deviations between T1 and T2 over the five tracks were 4.6 m and 2.4 m respectively; the corresponding Δx and Δy standard deviations between T1 and T3 were 3.1 m and 4.3 m, respectively. The mean of the differences Δx and Δy values between T1 and T2 over the five tracks and the corresponding ground truth had magnitudes of 2.8 m and 7.6 m, respectively; the corresponding means of the differences between T1 and T3 and the ground truth had magnitudes of 4.0 m and 0.6 m, respectively.

One criterion by which the performance of the algorithm is judged is the residual signal after all motion- and vehicle-induced noises and model target signals are removed. In this data analysis, we are observing residuals consistent with the nominal LSG noise floor operated in this system configuration using the current noise cancellation scheme. For example, the time series for the D magnetometer and the three signal differences for A – B, A – C, and A – D are displayed for one track in Fig. 4(b). The quality of the model fit for the A – D signal for the same track is displayed by the residual in Fig. 4(d) and its corresponding power spectrum in Fig. 4(e).

IV. SUMMARY AND FUTURE PLANS

The Polatomic LSG is a multi-channel scalar magnetometer-gradiometer designed for operation onboard AUVs with a 12-¾" outer diameter. Its operation is based on the electron-spin resonance (ESR) properties of helium-4 gas in accordance with the Zeeman effect, using a laser in place of incoherent light for optical pumping in order to increase sensitivity. It provides time series data for three independent scalar gradient channels and for the scalar magnetic field. A preliminary land-based sensor evaluation of the LSG has been completed.

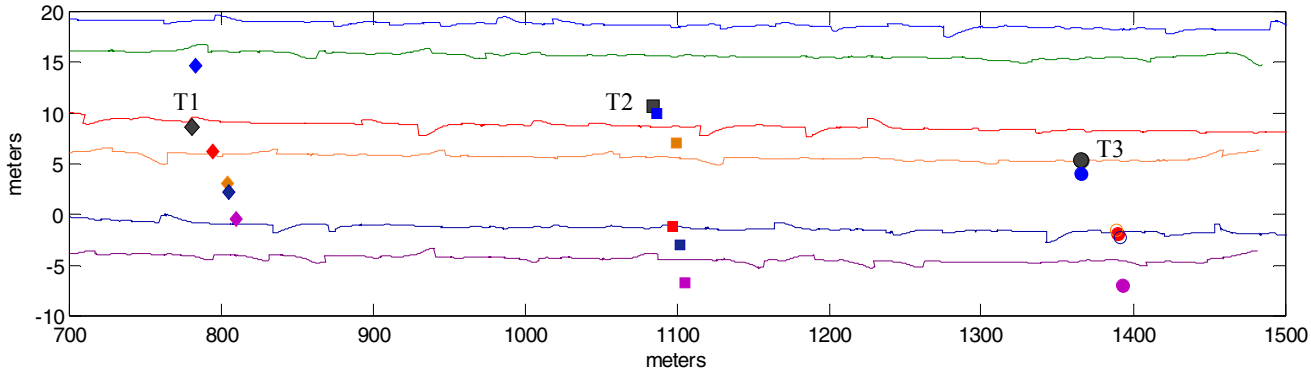

(a) Target localizations in six passes by targets T1, T2, and T3.

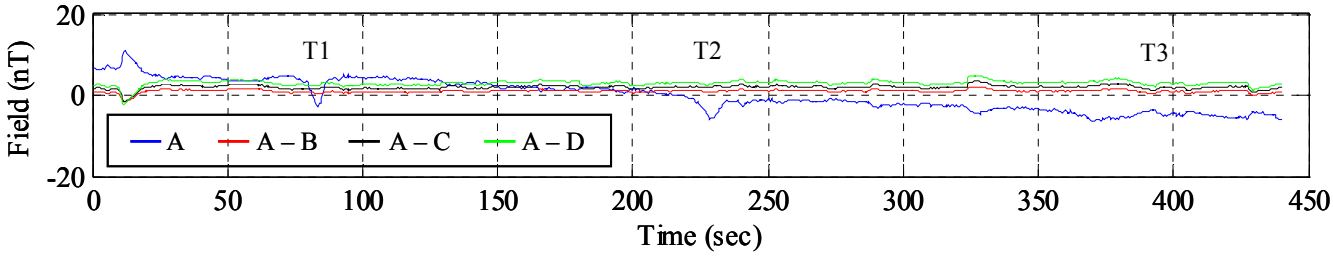

(b) Time series following data conditioning and filtering for magnetometer A and the signals differenced for A – B, A – C, and A – D.

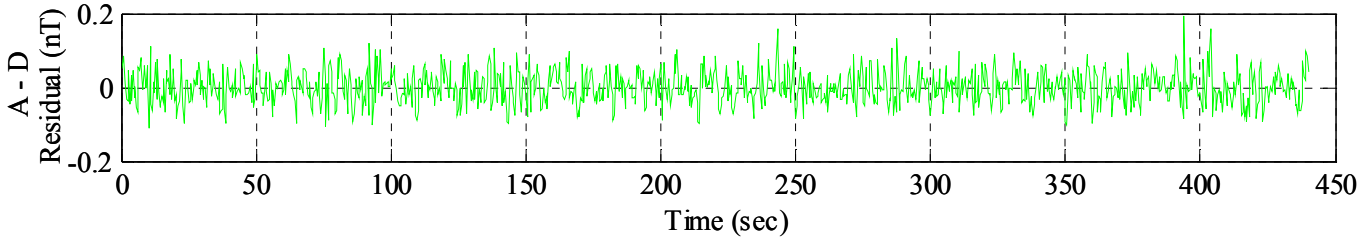

(c) Residual for the A – D difference after noise cancellation and model-target signal subtraction from the time series.

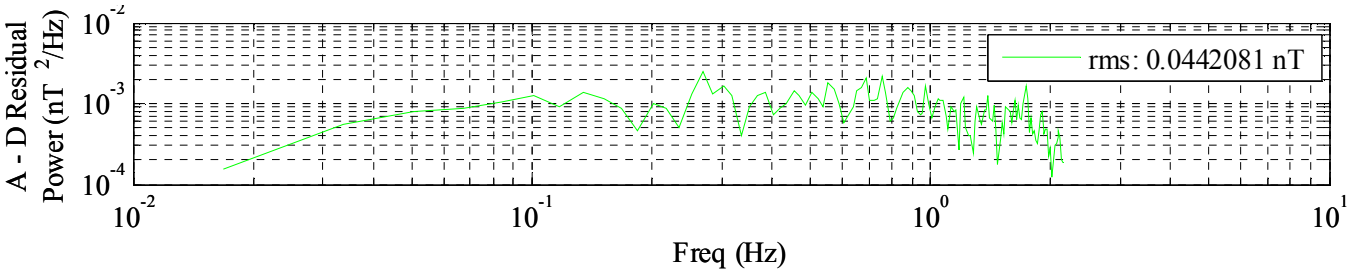

(d) Power spectrum for the residual signal for the A – D differenced signal.

Figure 4. Sample target localizations predicted by the LSG localization algorithm and related signal information from the data analysis.

The LSG has now been integrated into the REMUS 600 and this LSG-REMUS system has been tested underwater under operational conditions. Experiments have been conducted to measure LSG noise under operational conditions and to evaluate the LSG for target DCL. The noise floor ranges from 4×10^{-2} nT/(m-Hz$^{1/2}$) in the best case for the magnetometer pair most removed from the platform electromagnetic noise sources up to a figure on the order of 10^{-1} nT/(m-Hz$^{1/2}$) for pairs synthesized with cell A, the cell closest to the platform electromagnetic noise sources. The basic DCL algorithm for 5-channel tensor gradiometers has been modified for application to the scalar LSG and has been demonstrated in these experiments to detect and successfully localize targets.

Work continues in the near term to upgrade the LSG electronics to improve sensor performance with goals to

achieve a differenced single-cell magnetometer white noise floor of $6x10^{-4}$ $nT/Hz^{1/2}$ stationary, to reduce the power requirement for the LSG electronics and the affiliated internal heat buildup, to reduce thermal sensitivity, and to provide a more efficient cooling path to the LSG electronics. In parallel, work is in progress to modify the payload section, replace the active thermoelectric cooling with a passive cooling unit, and re-package the subsystems within the LSG payload section in order to reduce heat buildup and reduce electromagnetic noise internal to the LSG payload section. The results from the tests being reported in this paper are being analyzed to address discrepancies observed, to increase and optimize the effectiveness of the ancillary noise monitoring sensor network employed, to optimize the LSG localization algorithm including the affiliated noise-cancellation scheme, to address issues of data coregistration, and to improve operational procedures and reacquisition tactics. Additional testing of the LSG-REMUS system incorporating these modifications is planned for FY 2007.

The basic concept for an advanced version of the LSG far more compatible with AUV packaging has been developed that would implement several advances in the technology currently under development: fiber-optic (F-O) laser launching and Optically-driven Spin Precession (OSP) [4]. The F-O laser launching would permit each helium cell to be packaged in its own individual waterproof housing. Also, the cells would no longer have to be tightly mounted on a tubular superstructure to reinforce the rigidity, which is required to assure a precise optical path. Finally, the F-O technology permits configurations in which the LSG helium cells can be physically separated from the LSG laser and electronics in order to mitigate self-noise from the electronics.

The OSP technology will permit significant reduction of volume of the sense-cell assembly because intra-cell crosstalk, generated in the current LSG configuration using conventional Magnetically-driven Spin Precession (MSP), would no longer be a factor. The combination of the F-O and OSP technologies will allow convenient placement of the individual helium-cell packages, e.g. mounted in a compact tetrahedral configuration on the interior surface of the nose. With these advances, the payload section could be flooded and could be constructed no more than 24” long and 50 pounds dry, replacing the current dry payload section that is 76” long and weighs 350 pounds dry.

ACKNOWLEDGMENTS

The authors gratefully acknowledge the support from Dr. Kerry Commander, and Dr. Thomas Swean (ONR Code 321) who have made this work possible. The authors would also like to acknowledge the technical contributions to these efforts from our colleagues: Ben Allen, Ned Forrester, Amy Kukulya, Kwang Lee, Lang Nguyen, Keith Ostrom, Tim Pride, Alex Roup, Ray Vache, David Vandellen, Henry Van Wye, and Michael Wynn.

REFERENCES

[1] J.E. Piper and R. Lim, "Small object detection with a dual frequency synthetic aperture sonar," International Conference on Synthetic Aperture Sonar and Radar, Villa Marigola, Lerici, Italy, September 2006.

[2] S. G Schock, J. Wulf and J. Sara, "Imaging Performance of BOSS Using SAS Processing," published in these proceedings.

[3] G. Sulzberger, J. Bono, G.I. Allen, T. Clem, and S. Kumar, “Demonstration of the Real-Time Tracking Gradiometer for Buried Minehunting while Operating from a Small Unmanned Underwater Vehicle,” published in these proceedings.

[4] D. King, G. Kuhlman, and R. Slocum, “Polatomic Advances in Magnetic Sensors,” *MTS/IEEE Oceans 2002*, pp. 945-951, 2002.

[5] T. R. Clem P. S. Davis, R. J. McDonald, D. J. Overway, J. W. Purpura, L. Vaizer and D. King, “Preliminary Evaluation of the Laser Scalar Gradiometer For Buried Minehunting,” *MTS/IEEE OCEANS 2005*, Sep 2005.

[6] L. Vaizer, J. Lathrop, and J. Bono, “Localization of Magnetic Dipole Targets,” *MTS/IEEE Oceans 2004*, pp. 869-873, 2004.

[7] R. P. Stokey, A. Roup, C. von Alt, B. Allen, N. Forrester, T. Austin, R. Goldsborough, M. Purcell, F. Jaffre, G. Packard, and A. Kukulya, “Development of the REMUS 600 Autonomous Underwater Vehicle,” *MTS/IEEE OCEANS 2005*, Sep 2005

[8] K. H. Lee, unpublished results.

[9] J.S. Bendat and A.G. Piersol, *Engineering Applications of Correlation and Spectral Analysis,* Second Edition, Wiley Interscience, 1993.